HHS Public Access

Author manuscript

Ann Thorac Surg. Author manuscript; available in PMC 2017 January 30.

Published in final edited form as:

Ann Thorac Surg. 2015 October ; 100(4): 1360–1366. doi:10.1016/j.athoracsur.2015.03.096.

Saddle-Shaped Annuloplasty Improves Leaflet Coaptation in Repair for Ischemic Mitral Regurgitation

Wobbe Bouma, MD[*], **Chikashi Aoki, MD**[*], **Mathieu Vergnat, MD**, **Alison M. Pouch, PhD**, **Shanna R. Sprinkle, MD**, **Matthew J. Gillespie, MD**, **Massimo A. Mariani, MD, PhD**, **Benjamin M. Jackson, MD**, **Robert C. Gorman, MD**, and **Joseph H. Gorman III, MD**

Gorman Cardiovascular Research Group, University of Pennsylvania, Philadelphia, Pennsylvania; and University of Groningen, University Medical Center Groningen, Department of Cardiothoracic Surgery, Groningen, Netherlands

Abstract

Background—Current repair results for ischemic mitral regurgitation (IMR) with undersized annuloplasty rings are characterized by high IMR recurrence rates. Current annuloplasty rings treat annular dilatation, but they do little to improve (and may actually exacerbate) leaflet tethering. New saddle-shaped annuloplasty rings have been shown to maintain or restore a more physiologic annular and leaflet geometry and function. Using a porcine IMR model, we sought to demonstrate the influence of annuloplasty ring shape on leaflet coaptation.

Methods—Eight weeks after posterolateral infarct, eight pigs with grade 2+ or higher IMR were randomized to undergo either a 28-mm flat ring annuloplasty (n = 4) or a 28-mm saddle-shaped ring annuloplasty (n = 4). Real-time three-dimensional echocardiography and a customized image analysis protocol allowed three-dimensional assessment of leaflet coaptation before and after annuloplasty.

Results—Total leaflet coaptation area was significantly higher after saddle-shaped ring annuloplasty (109.6 ± 26.9 mm^2) compared with flat ring annuloplasty (46.2 ± 7.7 mm^2, $p < 0.01$). After annuloplasty, total coaptation area decreased by 87.5 mm^2 (or 65%) in the flat annuloplasty group ($p = 0.01$), whereas total coaptation area increased by 22.2 mm^2 (or 25%) in the saddle-shaped annuloplasty group ($p = 0.28$).

Conclusions—This study shows that the use of undersized saddle-shaped annuloplasty rings in mitral valve repair for IMR improves leaflet coaptation, whereas the use of undersized flat annuloplasty rings worsens leaflet coaptation. Because one of Carpentier's fundamental principles of mitral valve repair (durability) is to create a large surface of coaptation, saddle-shaped annuloplasty may increase repair durability.

Ischemic mitral regurgitation (IMR) is common, and its presence strongly affects prognosis [1, 2]. Even a mild degree of IMR adversely affects survival, with a strongly graded relationship between severity and reduced survival [1, 2]. In IMR the main pathophysiologic

Address correspondence to Dr Joseph H. Gorman, Gorman Cardiovascular Research Group, Smilow Center for Translational Research, 3400 Civic Center Blvd, Bldg 421, 11th Flr, Rm 112, Philadelphia, PA 19104-5156; gormanj@uphs.upenn.edu.

[*]Drs Bouma and Aoki contributed equally to this paper.

mechanism is ischemia-induced left ventricular (LV) remodeling with papillary muscle displacement and apical tethering or tenting of the mitral valve leaflets combined with annular dilatation and attenuation of the physiologic annular saddle shape [3]. Both annular dilatation (and flattening) (Carpentier type I dysfunction) and leaflet tethering (and flattening) (Carpentier type IIIb dysfunction) reduce leaflet coaptation and render the mitral valve insufficient [3]. Undersized ring annuloplasty does not address the main pathophysiologic mechanism of IMR, but it can provide reliable repair results by treating annular dilatation in patients with less advanced forms of LV dilatation and mitral valve tethering [4].

Although mitral valve repair with undersized ring annuloplasty, typically performed in conjunction with coronary artery bypass grafting, has become the preferred treatment [5, 6], the overall rate of IMR persistence and recurrence (moderate or severe IMR) remains high (up to 30% after 6 months and up to 60% after 3 to 5 years) [7, 8]. Undersized ring annuloplasty may potentiate leaflet tethering by displacing the posterior annulus anteriorly, which leads to increased posterior leaflet tethering [9]. Essentially, the mitral valve becomes functionally unileaflet. Leaflet tethering decreases leaflet curvature and results in increased leaflet and chordal stress [10]. The limited repair durability may explain the difficulty in demonstrating a survival benefit of annuloplasty for IMR [11].

The development of quantitative three-dimensional (3D) echocardiographic imaging has improved our understanding of mitral annular geometry [12, 13]. These new insights have led to the introduction of saddle-shaped annuloplasty rings to restore normal mitral annular 3D geometry. We have previously shown that saddle-shaped annuloplasty restores or maintains a more physiologic annular and leaflet geometry and function compared with flat annuloplasty [10, 14, 15] and that it reduces leaflet strain by increasing leaflet curvature [10, 14].

Based on this work we hypothesized that, despite the negative influence of undersized annuloplasty on leaflet coaptation, undersized saddle-shaped annuloplasty for IMR would promote a larger area of leaflet coaptation compared with undersized flat annuloplasty. To test this hypothesis we applied real-time 3D echocardiography and mitral valve tracing after mitral valve repair in a porcine IMR model.

Material and Methods

Surgical Protocol

The study protocol was reviewed and approved by the University of Pennsylvania School of Medicine Institutional Animal Care and Use Committee (IACUC) in Philadelphia and was in compliance with the *Guide for the Care and Use of Laboratory Animals* (US National Institutes of Health publication No. 85-23, revised 1996).

Eight adult male pigs were pretreated with buprenorphine (2 mg/kg); anesthesia was then induced with intravenous (IV) sodium thiopental (10 to 15 mg/kg), and the animals were intubated and anesthetized with isoflurane (1.5% to 2.0%) and oxygen. All animals received IV glycopyrrolate (0.02 mg/kg) and IV cefazolin (1.0 g). All animals underwent a right

thoracotomy to allow ligation of the left circumflex coronary artery and mid-posterior descending artery to create a 20% to 25% area of infarction [16]. Permanent occlusion of these arteries results in a transmural posterobasal myocardial infarction that involves approximately 20% to 25% of the LV mass and typically includes the entire posterior papillary muscle [16–18]. Animals received IV magnesium sulfate (1 g), IV amiodarone (90 mg by infusion over an hour), and IV lidocaine (3 mg/kg bolus, then 2 mg/min infusion) before infarction as antiarrhythmic prophylaxis. After hemodynamic and electrophysiologic stabilization, the thoracotomy was closed, and the animal was permitted to recover.

Eight weeks after infarction, animals were returned to the operating room. Anesthesia was once more induced, as described earlier, and all animals underwent epicardial echocardiography to assess the degree of IMR. All animals had grade 2+ or higher IMR. The mitral annulus was sized at 32 mm in all animals, and a 28-mm undersized annuloplasty ring (two sizes under) was used in each animal. Animals were randomized to undergo placement of a 28-mm flat mitral annuloplasty ring (Carpentier-Edwards Physio annuloplasty ring, Edwards Lifesciences, Irvine, CA) (Figs 1A, 1B) or to undergo placement of a 28-mm saddle-shaped mitral annuloplasty ring (Medtronic Profile 3D annuloplasty ring, Medtronic, Minneapolis, MN) (Figs 1C, 1D). Valve repair was performed through a left thoracotomy using cardiopulmonary bypass (CPB) and standard cardiac surgical techniques. The heart was arrested with antegrade cold crystalloid cardioplegia (PlegisolW, Hospira Inc, Lake Forest, IL), and the mitral valve was approached through a left atriotomy. After annuloplasty ring implantation the valve was tested in standard fashion and the atriotomy was closed, after which air was removed from the heart, and the animal was weaned from CPB. After separation from bypass and acquisition of epicardial echocardiographic data, animals were euthanized by an overdose of potassium administered into a clamped aortic root. After euthanasia, the heart was excised and the LV was opened through the interventricular septum. After repair inspection a digital photograph of the opened LV was taken and the infarct location was verified. All photographs were imported into an image analysis program (Image Pro Plus, MediaCybernetics; Silver Spring, MD), and computer-assisted planimetry was performed on the photographic image to quantify the infarct size as a percentage of the LV.

Echocardiographic Protocol

Full-volume data sets of the mitral valve were acquired using real-time 3D echocardiography with a Philips X7-2t handheld probe (Philips, Bothell, WA). Epicardial echocardiography was performed at the time of valve repair before instituting CPB and again after valve repair, approximately 1 hour after separation from bypass. All real-time 3D echocardiography studies were performed at an arterial systolic pressure of 150 mm Hg. Severity of IMR was determined semiquantitatively by assessing the area of the regurgitant jet as a percentage of left atrial area in the apical four-chamber view. The following grading scale was used: grade 0, no IMR; grade 1+, less than 20%; grade 2+, 20% to 40%; grade 3+, 40% to 60%; and grade 4+, more than 60% [19].

Image Segmentation

Each full-volume 3D data set was exported to an Echo-View 5.4 (TomTec Imaging Systems, Munich, Germany) software workstation. All analyses were performed at midsystole. The anterior and posterior commissures were defined as annular points at the junction between the anterior and posterior leaflets (middle of commissural region) and were interactively identified.

Techniques for mitral leaflet segmentation and modeling have been described previously [15]. Briefly, measurement planes were marked at 1-mm intervals along the entire length of the intercommissural axis (Fig 2A). In each two-dimensional (2D) plane, data points delineating anterior and posterior leaflets were traced across the atrial surfaces (Fig 2B), resulting in a 500- to 1,000-point data set for each valve.

For coaptation tracing, meticulous care was taken to clearly identify the tip of both anterior and posterior leaflets immediately before coaptation (using previous frames), so that the highest (most atrial) and lowest (most ventricular) margins of the coaptation zone could be defined. These atrial and ventricular edges of the coaptation zone (actual area of overlap) were then marked interactively (Fig 2B) [15].

The cartesian (X, Y, Z) coordinates of each data point were then exported from TomTec to Matlab software (The Mathworks, Natick, MA) to perform quantitative reconstruction.

Coaptation Analysis

Coaptation length was defined as the actual extent of overlap between the anterior and posterior leaflets (at a certain 2D cross-section). Any leaflet tissue beyond the line of apposition of two leaflets was not included as coaptation. Coaptation length was measured at 1-mm intervals spanning the entire mitral valve (from anterior to posterior commissure).

Coaptation area was defined as the area of overlap of the anterior and the posterior leaflets across the extent of the entire mitral valve (from anterior to posterior commissure). The 3D coaptation area was calculated using interpolation methods.

Segmental coaptation areas were determined by dividing the valve into equal thirds along the intercommissural axis. To provide a 2D visual representation of the coaptation area, the atrial and ventricular coaptation edges were projected onto a viewing plane orthogonal to the least squares annular plane passing through both commissures (Fig 2C) [15]. Averaged images were then created for each group by using interpolation of a normalized intercommissural sampling scale. The resulting images were centered for comparison.

Statistics

Continuous variables were expressed as mean ± standard deviation (SD). Comparisons between groups were performed using the independent-samples *t* test or Mann-Whitney *U* test (two-sided) as appropriate for continuous variables. Comparisons within groups were performed using the paired-samples *t* test or the Wilcoxon signed rank test (two-sided) as appropriate for continuous variables.

All calculations were performed using a commercially available statistical package (IBM SPSS Statistics 21.0; IBM Corporation, Chicago, IL). Statistically significant differences were established at $p < 0.05$.

Results

Perioperative Characteristics

Perioperative characteristics of animals in both annuloplasty groups are shown in Table 1.

Coaptation Area and Coaptation Length

Because of variations in the model and despite randomization, prerepair total leaflet coaptation area was significantly lower in the saddle-shaped annuloplasty group (87.4 ± 7.6 mm^2) compared with the flat annuloplasty group (133.7 ± 31.5 mm^2, $p = 0.03$). Despite this, total leaflet coaptation area was significantly higher after saddle-shaped ring annuloplasty (109.6 ± 26.9 mm^2) compared with flat ring annuloplasty (46.2 ± 7.7 mm^2, $p < 0.01$) (Table 2).

Figure 3 demonstrates a 2D projection of the averaged leaflet coaptation areas for each group. From this figure it can be seen that the coaptation area and coaptation lengths across the entire intercommissural distance are remarkably larger (especially in the A2-P2 and A3-P3 regions) for the saddle group than those of the flat group. The shape of the coaptation area was found to be different in both groups. The relationship of the coaptation lines and commissures to the annular plane is also illustrated. Notice how the flat ring tends to pull the commissures (especially the posterior commissure) and the coaptation lines in a more atrial direction.

A comparison of postoperative change in coaptation length (and area) as a function of normalized intercommissural position is shown in Figure 4. After annuloplasty, total coaptation area decreased by 87.5 mm^2 (or 65%; from 133.7 mm^2 to 46.2 mm^2) in the flat annuloplasty group ($p = 0.01$), whereas total coaptation area increased by 22.2 mm^2 (or 25%; from 87.4 mm^2 to 109.6 mm^2) in the saddle-shaped annuloplasty group ($p = 0.28$). In the flat annuloplasty group, coaptation length decreased after repair in all regions, whereas in the saddle-shaped annuloplasty group, coaptation length increased after repair in all regions. Notice the largest decrease in postrepair coaptation length for the flat annuloplasty group in the A2-P2 region and the largest increase in postrepair coaptation length for the saddle-shaped annuloplasty group in the A2-P2 and A3-P3 regions.

Comment

Carpentier's three fundamental principles of durable mitral valve repair are (1) to preserve or restore full leaflet motion, (2) to create a large surface of coaptation, and (3) to remodel and stabilize the entire annulus [20]. The factors that influence coaptation are annular size, annular shape, and the amount of mobile leaflet tissue. The first two factors can be altered with ring annuloplasty, and the third factor can be changed by a growing number of new surgical techniques. Annular reduction for IMR with undersized flat annuloplasty improves leaflet coaptation by reducing annular size, but at the same time it impedes coaptation (as

shown in Fig 3 of this study) by exacerbating posterior leaflet tethering [9]. As shown in Figure 3, the flat ring elevates ("atrializes") the leaflet commissures. This atrialization can potentially exacerbate posterior leaflet tethering [15, 21]. Flat annuloplasty rings have also been shown to decrease posterior leaflet mobility in IMR [22], thus resulting in a functionally unileaflet (monocusp) valve with displacement of coaptation toward the posterior annulus [21, 23] and the annular plane [21]. Taken together, after undersized flat annuloplasty for IMR, different mechanisms may cause increased tethering and reduced coaptation (with augmented leaflet and annular strain), which predispose to IMR recurrence and repair failure.

During the past decade we have been able to quantify the normal saddle shape of the mitral valve by using a variety of imaging modalities [13, 24, 25] and document the importance of this shape in optimal valve performance [10]. These findings have led to the introduction of a new generation of saddle-shaped annuloplasty rings, which have been shown to maintain more physiologic patterns of annular and leaflet geometry compared with flat rings [14, 26, 27]. On the basis of these studies we hypothesized that, despite the negative influence of undersized annuloplasty on leaflet coaptation, undersized saddle-shaped annuloplasty for IMR would have a strong beneficial influence on leaflet coaptation.

IMR repair failure continues to be a significant clinical problem. Failure mechanisms can be, at least partially, attributable to leaflet tethering and stress with reduced coaptation. The results of this study are both counterintuitive and compelling. Although it is likely that undersized saddle-shaped annuloplasty for IMR increases leaflet tethering by "the undersizing mechanism," it seems that preserving the saddle shape augments leaflet coaptation by maintaining the normal commissural positions and line of coaptation and as a result may have a beneficial influence on repair durability. This finding corroborates previous work that has shown improved coaptation after saddle-shaped annuloplasty in degenerative mitral valve disease [15].

Real-time 3D echocardiography improves our understanding of the influence of annuloplasty on postrepair mitral leaflet coaptation and literally takes it to a new dimension. Real-time 3D echocardiography combined with our image analysis algorithms provides a superior tool for quantifying the influence of annuloplasty and other repair techniques on the complex and dynamic geometry of the entire mitral valve. Unlike 2D echocardiography, this method is not influenced by viewing plane selection, regional asymmetry, or annular distortions and therefore represents a clinically relevant and consistent technique for quantitative in vivo assessment of mitral valve disease and repair. One limitation of this technique is the need for time-consuming off-line analysis. Therefore, work is in progress to develop automated segmentation techniques that will allow image processing and mitral leaflet segmentation in minutes rather than hours [28].

Figure 3 graphically compares leaflet coaptation length across the entire coaptation zone in both groups. This figure demonstrates regional heterogeneity in the difference in coaptation length between the two groups. The saddle ring most profoundly augments coaptation length in the A2-P2 and A3-P3 regions. From Figure 4 it becomes clear that the flat ring most profoundly reduces coaptation length in the A2-P2 region. Both figures highlight the

strength of our 3D imaging methodology. The technique is not influenced by asymmetry of leaflet closure or coaptation along the mitral valve and therefore overcomes many of the limitations of 2D imaging.

Despite the compelling results, further investigation is necessary to correlate postrepair coaptation area with leaflet curvature and stress distributions and to follow the long-term outcome of patients with IMR who are treated with saddle-shaped annuloplasty rings. Because the pathologic 3D anatomy of IMR is complex and varies extensively among patients [15], future research should also focus on quantitatively determining the relative contribution of annular dilatation and leaflet tethering to IMR in the individual patient. This would help surgeons decide among valve replacement, simple repair with annuloplasty alone, or a combined approach with more complex leaflet or subvalvular repair techniques. Saddle-shaped annuloplasty remains an annular solution to a predominantly subvalvular problem, which may eventually render it prone to IMR recurrence. Subvalvular techniques that promote LV (reverse) remodeling should be an equally important focus in the treatment of IMR.

Compared with the 28-mm flat ring, a 28-mm saddle-shaped ring provides a slightly larger inner commissure-to-commissure diameter (27.8 versus 26.6 mm), but a 2.3-mm smaller inner septolateral diameter (15.4 versus 17.7 mm) [29]. Additional septolateral undersizing of a 28-mm saddle-shaped ring may have improved coaptation and could have biased conclusions about the true influence of saddle-shaped annuloplasty on coaptation. Although undersizing can improve coaptation by annular reduction, it can also increase posterior leaflet tethering and reduce coaptation [9, 15, 21]. In addition to annular shape, annular size and total leaflet area both influence leaflet coaptation area. That leaflet coaptation area was not normalized to postrepair mitral annular area and total leaflet area in this study can be considered a limitation. The “accidental” heterogeneity in prerepair coaptation area between the two groups actually added strength to the study.

To conclude, this study shows that the use of undersized saddle-shaped annuloplasty rings in mitral valve repair for IMR improves leaflet coaptation, whereas the use of undersized flat annuloplasty rings worsens leaflet coaptation. Because one of Carpentier’s fundamental principles of mitral valve repair (durability) is to create a large surface of coaptation, saddle-shaped annuloplasty may increase repair durability. The proposed efficacy of saddle-shaped annuloplasty on mitral valve repair durability is speculative, but it is compelling in the light of a growing body of work by our group and others that supports the positive influence of annular saddle shape on valve stress-strain profiles and leaflet coaptation.

Acknowledgments

This research project was supported by grants from the National Heart, Lung and Blood Institute of the National Institutes of Health (HL63954 and HL73021). It was also supported by an investigator-initiated grant from Medtronic. Robert Gorman and Joseph Gorman were supported by Individual Established Investigator Awards from the American Heart Association.

Abbreviations and Acronyms

2D	two-dimensional

3D	three-dimensional
CPB	cardiopulmonary bypass
IMR	ischemic mitral regurgitation
IV	intravenous
LV	left ventricular

References

1. Trichon BH, Felker GM, Shaw LK, Cabell CH, O'Conner CM. Relation of frequency and severity of mitral regurgitation to survival among patients with left ventricular systolic dysfunction and heart failure. Am J Cardiol. 2003; 91:538–543. [PubMed: 12615256]
2. Grigioni F, Enriquez-Sarano M, Zehr KJ, Bailey KR, Tajik AJ. Ischemic mitral regurgitation: long-term outcome and prognostic implications with quantitative Doppler assessment. Circulation. 2001; 103:1759–1764. [PubMed: 11282907]
3. Bouma W, van der Horst ICC, Wijdh-den Hamer IJ, et al. Chronic ischaemic mitral regurgitation: current treatment results and new mechanism-based surgical approaches. Eur J Cardiothorac Surg. 2010; 37:170–185. [PubMed: 19716310]
4. Braun J, van de Veire NR, Klautz RJ, et al. Restrictive mitral annuloplasty cures ischemic mitral regurgitation and heart failure. Ann Thorac Surg. 2008:430–436. [PubMed: 18222238]
5. Gillinov AM, Wierup PN, Blackstone EH, et al. Is repair preferable to replacement for ischemic mitral regurgitation? J Thorac Cardiovasc Surg. 2001; 122:1125–1141. [PubMed: 11726887]
6. Grossi EA, Goldberg JD, LaPietra A, et al. Ischemic mitral valve reconstruction and replacement: comparison of long-term survival and complications. J Thorac Cardiovasc Surg. 2001; 122:1107–1124. [PubMed: 11726886]
7. McGee EC, Gillinov AM, Blackstone EH, et al. Recurrent mitral regurgitation after annuloplasty for functional ischemic mitral regurgitation. J Thorac Cardiovasc Surg. 2004; 128:916–924. [PubMed: 15573077]
8. Hung J, Papakostas L, Tahta SA, et al. Mechanism of recurrent ischemic mitral regurgitation after annuloplasty: continued LV remodeling as a moving target. Circulation. 2004; 110:II85–II90. [PubMed: 15364844]
9. Kuwahara E, Otsuji Y, Iguro Y, et al. Mechanism of recurrent/persistent ischemic/functional mitral regurgitation in the chronic phase after surgical annuloplasty: importance of augmented posterior leaflet tethering. Circulation. 2006; 114:I529–I534. [PubMed: 16820632]
10. Salgo IS, Gorman JH 3rd, Gorman RC, et al. Effect of annular shape on leaflet curvature in reducing mitral leaflet stress. Circulation. 2002; 106:711–717. [PubMed: 12163432]
11. Mihaljevic T, Larn BK, Rajeswaran J, et al. Impact of mitral valve annuloplasty combined with revascularization in patients with functional ischemic mitral regurgitation. J Am Coll Cardiol. 2007; 49:2191–2201. [PubMed: 17543639]
12. Jassar AS, Brinster CJ, Vergnat M, et al. Quantitative mitral valve modeling using real-time three-dimensional echocardiography: technique and repeatability. Ann Thorac Surg. 2011; 91:165–171. [PubMed: 21172507]
13. Ryan LP, Jackson BM, Enomoto Y, et al. Description of regional mitral annular non-planarity in normal human subjects: a novel methodology. J Thorac Cardiovasc Surg. 2007; 134:644–648. [PubMed: 17723812]
14. Ryan LP, Jackson BM, Hamamoto H, et al. The influence of annuloplasty ring geometry on mitral leaflet curvature. Ann Thorac Surg. 2008; 86:749–760. [PubMed: 18721556]
15. Vergnat M, Jackson BM, Cheung AT, et al. Saddle-shape annuloplasty increases mitral leaflet coaptation after repair for flail posterior leaflet. Ann Thorac Surg. 2011; 92:797–803. [PubMed: 21803330]

16. Witschey WR, Pila JJ, Ferrari G, et al. Rotating frame spin lattice relaxation in a swine model of chronic, left ventricular myocardial infarction. Magn Reson Med. 2010; 64:1453–1460. [PubMed: 20677236]
17. Guy TS 4th, Moainie SL, Gorman JH 3rd, et al. Prevention of ischemic mitral regurgitation does not influence the outcome of remodeling after posterolateral myocardial infarction. J Am Coll Cardiol. 2004; 43:377–383. [PubMed: 15013117]
18. Llaneras MR, Nance ML, Streicher JT, et al. Large animal model of ischemic mitral regurgitation. Ann Thorac Surg. 1994; 57:432–439. [PubMed: 8311608]
19. Miyatake K, Izumi S, Okamoto M, et al. Semiquantitative grading of severity of mitral regurgitation by real-time two-dimensional Doppler flow imaging technique. J Am Coll Cardiol. 1986; 7:82–88. [PubMed: 3941221]
20. Carpentier, A., Adams, DH., Filsoufi, F. Philadelphia: Saunders; 2010. Carpentier's reconstructive valve surgery; p. 64
21. Jensen MO, Jensen H, Levine RA, et al. Saddle-shaped mitral valve annuloplasty rings improve leaflet coaptation geometry. J Thorac Cardiovasc Surg. 2011; 142:697–703. [PubMed: 21329946]
22. Green GR, Dagum P, Glasson JR, et al. Restricted posterior leaflet motion after mitral ring annuloplasty. Ann Thorac Surg. 1999; 68:2100–2106. [PubMed: 10616984]
23. Gogoladze G, Dellis SL, Donnino R, et al. Analysis of the mitral coaptation zone in normal and functional regurgitant valves. Ann Thorac Surg. 2010; 89:1158–1161. [PubMed: 20338324]
24. Gorman JH III, Gupta KB, Streicher JS, et al. Dynamic three-dimensional imaging of the mitral valve using rapid sonomicrometry array localization. J Thorac Cardiovasc Surg. 1996; 112:712–725. [PubMed: 8800160]
25. Gorman JH III, Jackson BM, Enomoto Y, Gorman RC. The effect of regional ischemia on mitral valve annular saddle shape. Ann Thorac Surg. 2004; 77:544–548. [PubMed: 14759435]
26. Mahmood F, Subramanian B, Gorman JH III, et al. Three-dimensional echocardiographic assessment of changes in mitral valve geometry after valve repair. Ann Thorac Surg. 2009; 88:1838–1844. [PubMed: 19932245]
27. Mahmood F, Gorman JH III, Subramanian B, et al. Changes in mitral valve annular geometry after repair saddle shaped vs. flat annuloplasty rings. Ann Thorac Surg. 2010; 90:1212–1220. [PubMed: 20868816]
28. Pouch AM, Wang H, Takabe M, et al. Fully automatic segmentation of the mitral leaflets in 3D transesophageal echocardiographic images using multi-atlas joint label fusion and deformable medial modeling. Med Image Anal. 2014; 18:118–129. [PubMed: 24184435]
29. Bothe W, Swanson JC, Ingels NB, Miller DC. How much septal-lateral mitral annular reduction do you get with new ischemic/functional mitral regurgitation annuloplasty rings? J Thorac Cardiovasc Surg. 2010; 140:117–121. [PubMed: 20074748]

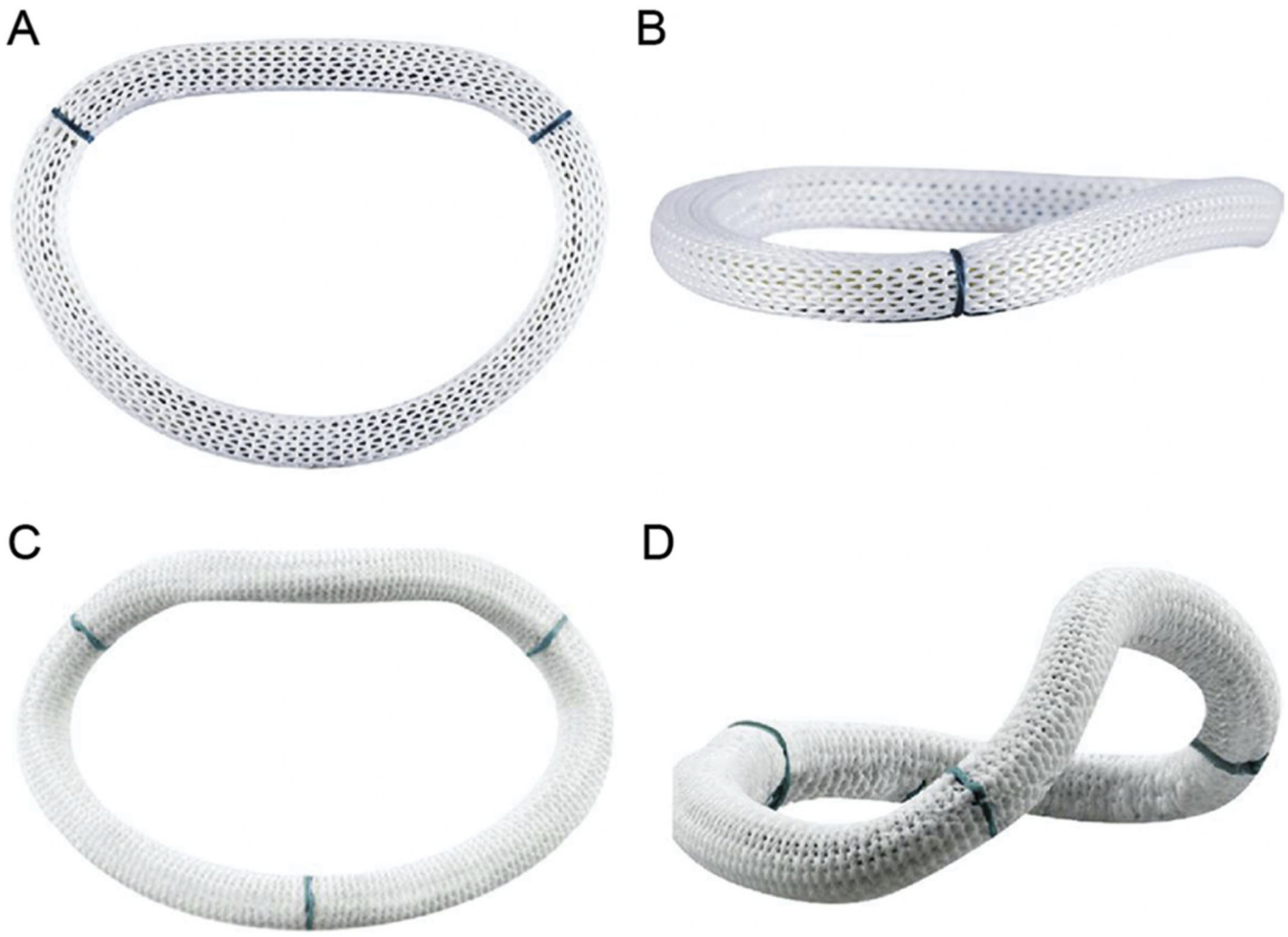

Fig 1.

Mitral annuloplasty rings viewed from different orientations. (A) and (B) Carpentier-Edwards Physio (Edwards Lifesciences, Irvine, CA) flat mitral annuloplasty ring. (C) and (D) Medtronic Profile 3D (Medtronic, Minneapolis, MN) saddle-shaped mitral annuloplasty ring. Subtle differences in the shape of the flow orifice can be appreciated in the short-axis views (A and C), whereas dramatic differences in annular height and nonplanarity are evident in the oblique views (B and D).

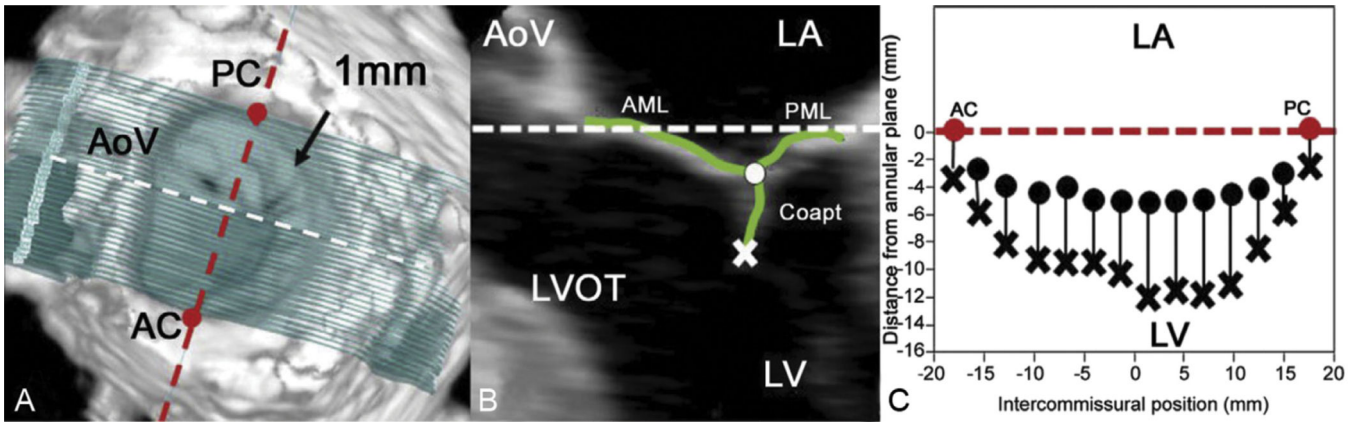

Fig 2.

Leaflet segmentation technique. (A) Template of transverse cross-sections every 1 mm along the intercommissural axis. (B) One of the two-dimensional cross-sections represented by the white dashed line in (A); the atrial surface of the mitral valve leaflets and the coaptation zone are interactively marked (green curves). The most atrial coaptation point is marked with the white dot, and the most ventricular coaptation point is marked with an X. (C) Schematic demonstrating how the atrial and ventricular coaptation points are then projected onto a viewing plane orthogonal to the least squares annular plane passing through the commissures to construct a two-dimensional representation of the coaptation zone. The white and red dashed lines are both within least squares annular plane in all three panels. (AC = anterior commissure; AML = anterior mitral leaflet; AoV = aortic valve; Coapt = coaptation; LA = left atrium; LV = left ventricle; LVOT = left ventricular outflow tract; PC = posterior commissure; PML = posterior mitral leaflet.)

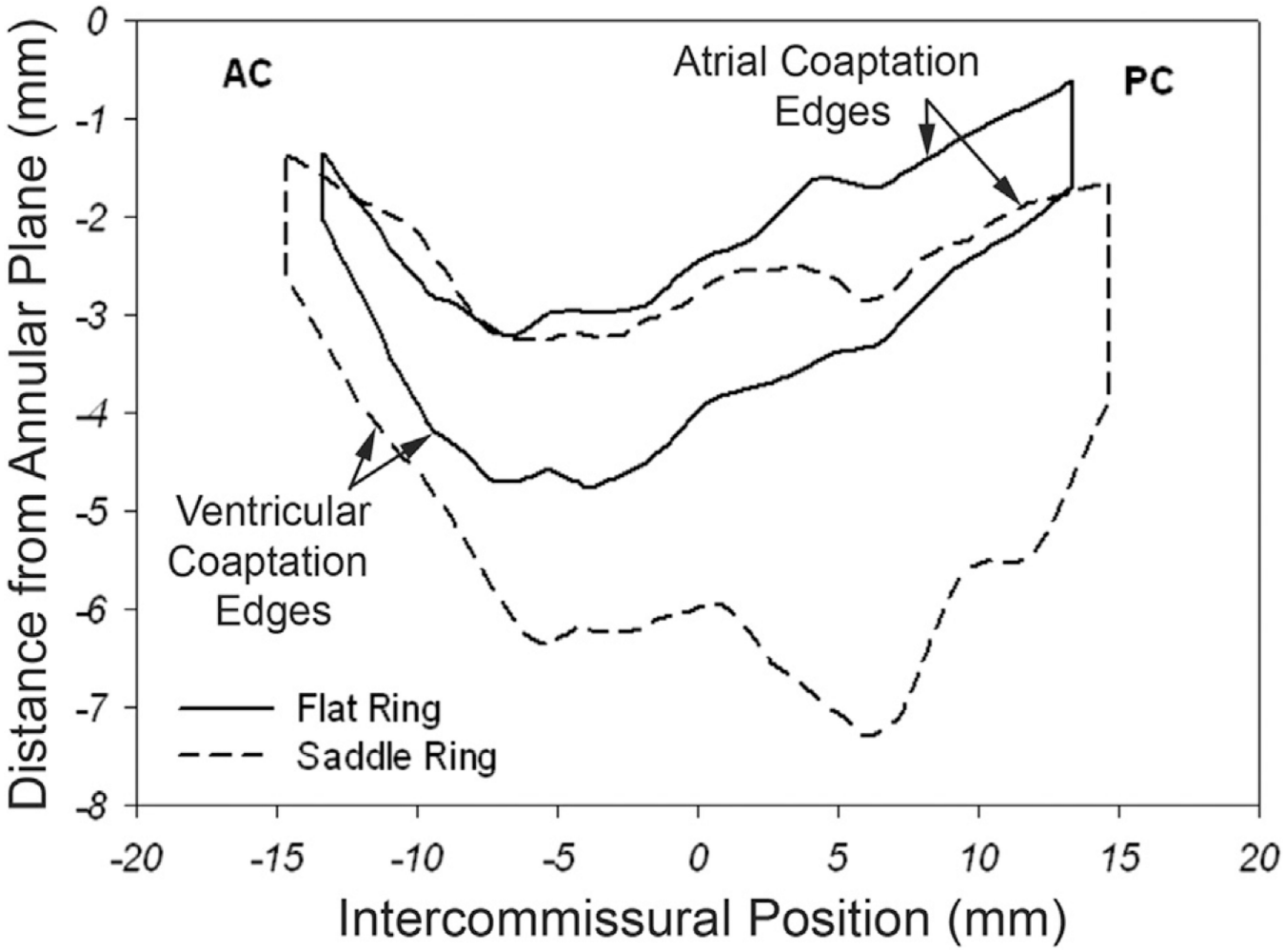

Fig 3.

Comparison of coaptation area and coaptation length. The black curve represents the two-dimensional projections of the averaged atrial and ventricular coaptation edges for the flat annuloplasty group. The area bounded by the two curves is the projected two-dimensional coaptation area. The distance between the two curves represents coaptation length at each intercommissural position. The dashed curve signifies similar parameters for the saddle-shaped annuloplasty group. The represented viewing plane is orthogonal to the averaged best-fit annular plane and passes through the line connecting the anterior commissure (AC) and the posterior commissure (PC). These composite images were created using interpolation of a normalized intercommissural sampling scale for each valve.

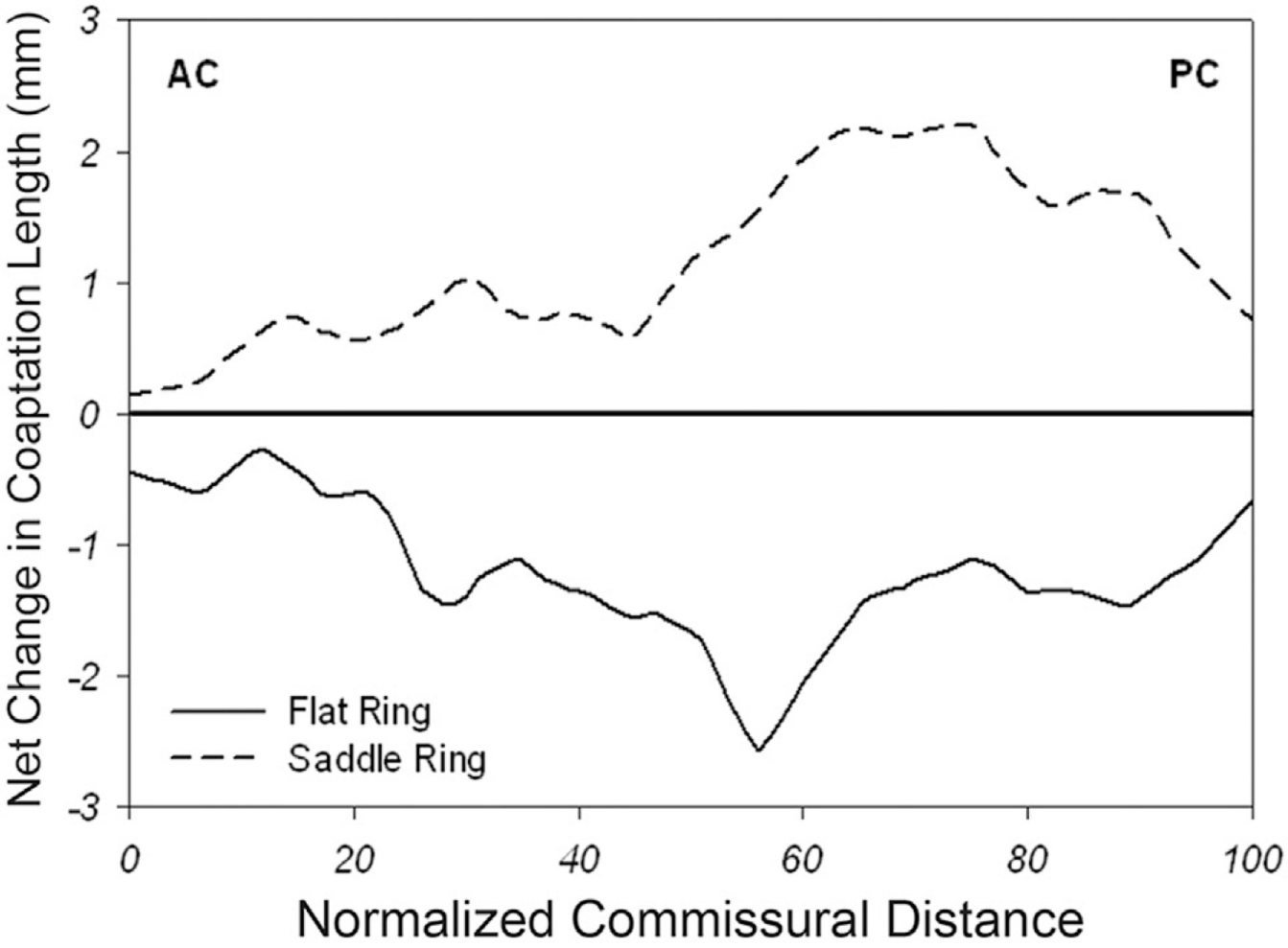

Fig 4.

Comparison of postoperative change in coaptation length (and area). Shown here is net change in coaptation length (postrepair coaptation length compared with prerepair coaptation length) versus normalized intercommissural position for both the saddle-shaped (dashed) and flat (black) annuloplasty groups. Notice an increase in coaptation length (and area) across the entire intercommissural distance for the saddle group (especially toward the posterior commissure [PC]) and a decrease in coaptation length (and area) across the entire intercommissural distance for the flat group (especially toward the PC). (AC = anterior commissure.)

Table 1

Perioperative Characteristics

Parameter[a,b]	Flat Ring (n = 4)	Saddle Ring (n = 4)
Body weight, kg	58.8 ± 6.8	58.5 ± 10.8
Heart weight, g	339.5 ± 6.8	366.8 ± 49.3
Infarction area, %	28.5 ± 8.7	22.1 ± 4.2
Preoperative EF, %	26.3 ± 2.5	27.5 ± 2.9
Preoperative IMR grade	3.3 ± 1.0	3.0 ± 1.0
CPB time, min	188.5 ± 78.4	169.7 ± 45.5
ACC time, min	100.0 ± 30.6	113.0 ± 19.7
Postoperative IMR grade	0.5 ± 1.0	0.0 ± 0.0

[a] Data are presented as mean ± standard deviation.

[b] No significant between-group differences ($p > 0.05$).

ACC = aortic-cross-clamp; CPB = cardiopulmonary bypass; EF = ejection fraction; IMR = ischemic mitral regurgitation.

Table 2

Coaptation Parameters

Parameter[a]	Flat Ring (n = 4)	Saddle Ring (n = 4)
Prerepair total coaptation area, mm^2	133.7 ± 31.5	87.4 ± 7.6[b]
Prerepair segmental coaptation area, mm^2		
A1-P1	35.2 ± 8.9	26.0 ± 2.8
A2-P2	55.4 ± 19.8	32.0 ± 3.0
A3-P3	43.2 ± 4.0	29.4 ± 4.7[b]
Postrepair total coaptation area, mm^2	46.2 ± 7.7[c]	109.6 ± 26.9[b]
Postrepair segmental coaptation area, mm^2		
A1-P1	15.3 ± 5.0[c]	29.7 ± 9.1[b]
A2-P2	16.5 ± 2.4[c]	42.2 ± 15.3[b]
A3-P3	14.4 ± 3.8[c]	37.6 ± 13.0[b]

[a] Data are presented as mean ± standard deviation.

[b] Significant between-group difference (saddle versus flat) ($p < 0.05$).

[c] Significant within-group difference (postrepair versus prerepair) ($p < 0.05$).